Microwave Journal®

Optimizing D-Band Amplifiers: Diving Into RF Measurement Challenges

COVER FEATURE
INVITED PAPER

A. Engelmann*, B. Derat**, M. Lörner** and M. Dietz***
*Institute for Smart Electronics and Systems (LITES), Friedrich-Alexander-Universität, Erlangen, Germany
**Rohde & Schwarz, Munich, Germany
***Fraunhofer Institute, Electronic Microsystems and Solid-State Technology (EMFT), Munich, Germany

RF characterization up to D-Band (110 to 170 GHz) is increasingly necessary with the current drive toward 6G wireless communications, high speed digital links and advanced sensing technologies. Considering the sensing use case and the design and optimization of a D-Band power amplifier (PA), this article investigates the measurement challenges accompanying leading-edge RF technology development. The importance of measuring amplifiers with actual load conditions in an on-wafer test environment will be illustrated.

MMWAVE SINGLE-CONNECT IS THE NEW NORMAL

In 1950, Rohde & Schwarz achieved a remarkable milestone: creating the first vector network analyzer (VNA). This instrument characterized single-port S-parameters to 300 MHz, a breakthrough in RF measurements. Seventy-five years of technological development later, RF design and testing have evolved to where mmWave characterization is the new normal. A single measurement setup captures more than S-parameters and provides a complete performance overview of the device under test (DUT) after one calibration and connection.

Single-touchdown is of the utmost relevance to IC design where costly and fragile die are measured with delicate probing systems. RF components and modules, typically made for matching 50 Ω conditions, are now used in complex, non-ideal environments. It is a common requirement for semiconductor foundries to provide 50 Ω reference specifications and accurate models to enable system integrators and IC designers to achieve the best system performance.

This article discusses challenges in large-signal characterization of D-Band PAs using a sub-THz load-tuning measurement setup.

D-BAND AMPLIFIER FOR SENSING APPLICATIONS

Large channel bandwidths in D-Band create new possibilities for high-resolution imaging, radar and high data-rate communication systems. PAs are a key building block in these applications and are used before transmit chain antennas or as a driver stage for a frequency multiplier or mixer. Advanced silicon-on-insulator (SOI) CMOS technologies achieving an f_T and f_{max} of 350 GHz and 370 GHz, respectively, are suitable for low-power, high efficiency mmWave circuits. Despite the high performance of mmWave transistors, achieving high output power at D-Band frequencies is still challenging. The short gate length, which results in low operational and breakdown voltages, is a critical output power limiting factor.

Using transistors with longer gate widths and higher current swings can increase output power. However, this creates a significant gain reduction at high frequencies, caused mainly by increased parasitic gate-drain and gate-source capacitance. Enlarging the transistor gate width also decreases the optimum output impedance. The transformation ratio to 50 Ω becomes larger and may lead to lossier matching networks. Power-combining is a common approach to increase output power.

However, this requires additional complex dividers and combining structures, increasing loss, DC power and chip area.[1,2] SOI technology enables transistor stacking to increase the maximum voltage swing, which has already been successfully demonstrated at lower frequencies.[3] Nevertheless, this amplifier topology requires an increased nominal supply voltage, which can require special care and have disadvantages for integration into larger systems.

Two implementations of com-

Reprinted with permission of MICROWAVE JOURNAL® from the March 2025 issue.
©2025 Horizon House Publications, Inc.

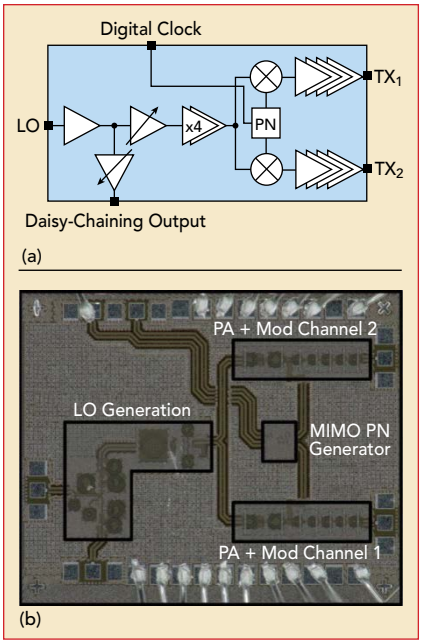

Fig. 1 **PMCW transmitter block diagram (a) and transmitter chip micrograph (b).**

pact, energy-saving and high efficiency D-Band PAs have been proposed.[4] These PAs operate at 0.8 V supply voltage on 22 nm fully-depleted SOI (FD-SOI) technology. The PAs are part of a gesture/motion recognition in a phase-modulated continuous wave (PMCW) radar transceiver system. This emerging application allows new man-machine interfaces and supports non-invasive vital sign assessment. The radar architecture was introduced by F. Probst et al.[5] ***Figure 1*** shows the Tx architecture and a micrograph of the chip and the relevant building blocks. Two broadband transmit antennas and the Tx chip are integrated into an embedded wafer-level ball grid array (eWLB) package.

The antenna/Tx interconnection has significant losses at D-Band frequencies. Chip placement and subsequent processing of the antenna redistribution layers are highly dependent on process tolerances, creating modeling and interconnection challenges. The PA design ensures sufficient output power to the antennas, even when manufacturing tolerances change antenna input impedances. Load sensitivity simulations and measurements are necessary to evaluate this essential capability of the PA.

The amplifier stages employ a pseudo-differential topology. ***Figure 2*** shows the differential common-source transistor pair schematic with cross-coupled neutralization capacitors (C_N). These capacitors boost gain and increase differential mode stability by compensating for the parasitic gate-drain capacitance (C_{gd}). C_N overcompensates C_{gd}, resulting in a three to four dB gain increase instead of maximizing stability. Figure 2 shows the C_N influence on the maximum available gain (G_{max}), K and μ stability factors at 140 GHz. To limit compensation network losses, C_N are alternated polarity metal-oxide-metal (APMOM) capacitors. The back-gate bias voltage feeds two resistors, R_{BG} and aids operation point tuning.

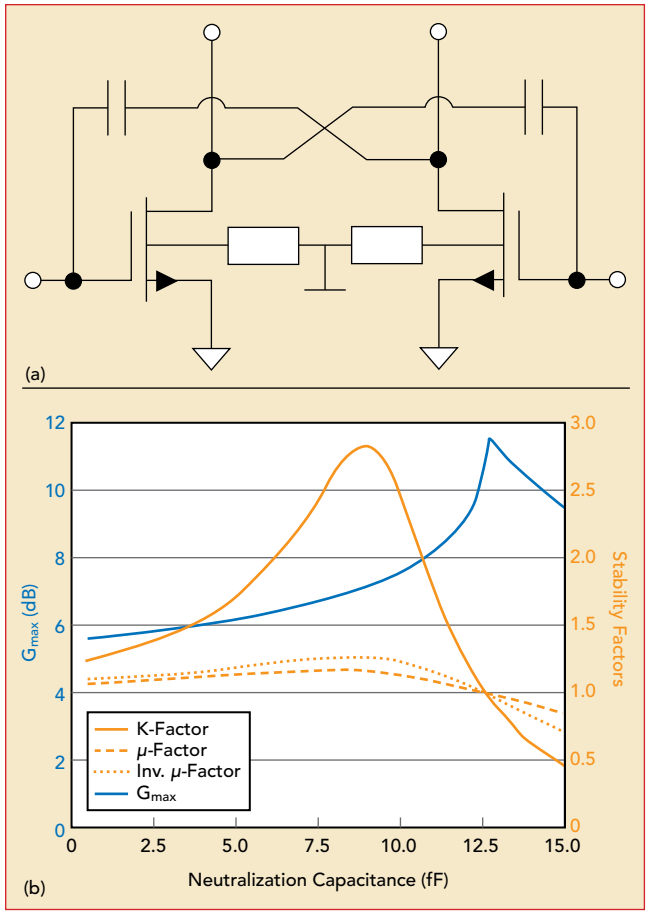

Fig. 2 **Pseudo-differential topology (a) and 140 GHz performance (b).**

Each PA has three drivers for sufficient gain and one high-power output stage. ***Figure 3*** shows a simplified block diagram of the two PAs. Tuning the driver gain to slightly different frequencies enhances amplifier bandwidth, while load-pull simulations optimize the output-matching network to maximize the available output power. Each stage uses super-low threshold voltage (SLVT) n-MOS transistors with double gate-pitch, double-sided gate connection and minimum channel length of 20 nm. Two parallel, 600 nm finger-width transistors are used as driver stages to account for the gate resistance/parasitic finger capacitance trade-off. Three parallel 800 nm finger-width transistors comprise the output stages. Output PA stages are biased for class AB operation for better efficiency, while the drivers are biased in class A for high gain. Two mmWave implementation methods were investigated for the input, output and interstage matching networks. The first uses stacked transformer-based (TB) matching, while the second uses T-line-based (LB) networks.

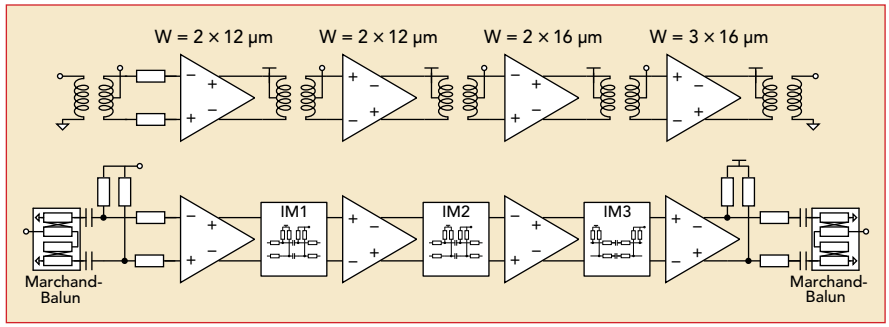

Fig. 3 **TB-PA (top) and LB-PA (bottom).**

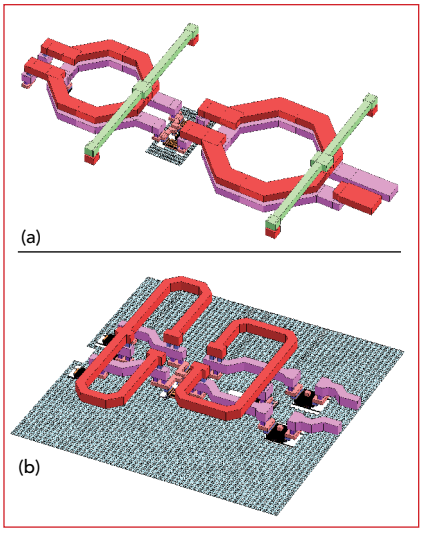

Fig. 4 **Input- and output-matching networks of the TB-PA (a) and LB-PA (b).**

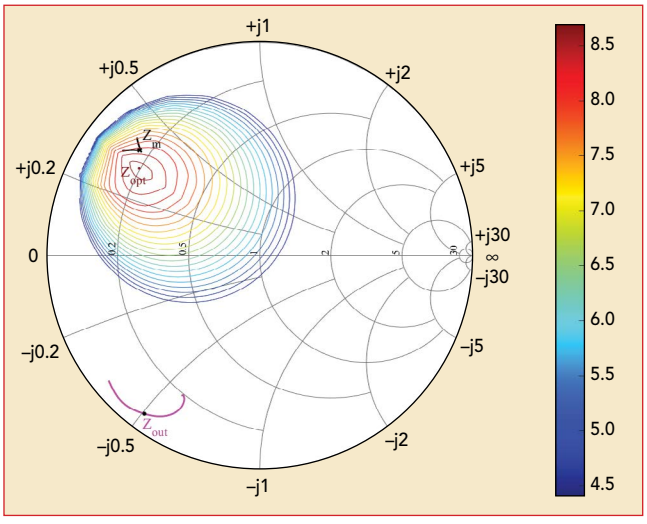

Fig. 5 **Simulated 140 GHz load-pull power contours.**

Figure 4 shows 3D views of the TB-PA and LB-PA output stages. The TB-PA benefits from the transformer's compact device size and the ease of routing the DC feed over the center tabs. Short T-lines between the input transformer and the first PA stage provide more efficient impedance matching. For measurement purposes, input and output transformers are baluns. The main drawback of this design is the increased effort to generate accurate circuit models encompassing all relevant D-Band parasitic effects.

The LB-PA implementation benefits from less complex T-line device modeling and more straightforward modular design flows. Taking advantage of the differential circuit's symmetry and the two available thick copper layers, the shorted T-line stubs can be rolled up, as shown in Figure 4. This layout results in a compact design and the LB matching network dimensions are comparable to the TB realization. The symmetry points provide good DC bias and supply voltage feed connections. Additional capacitors are inserted between stages to separate gate bias and supply voltage feeds, resulting in additional matching network losses. Another drawback is the necessity of auxiliary components for single-ended-to-differential conversion required for on-wafer measurements. This requires broadband Marchand baluns at the LB-PA input and output, resulting in extra chip area and increasing fabrication cost.

Load-pull simulations determine the optimal PA matching impedance. ***Figure 5*** shows the 140 GHz load-pull simulation results for the TB-PA output stage. The maximum achievable output power of the stage at the optimal load point, Z_{opt}, is 8.7 dBm. The output impedance, Z_{out}, of the PA stage and the input impedance of the matching balun, Z_m, are displayed over frequency with a 140 GHz marker. The matching balun brings the 50 Ω load close to the optimum load point but introduces approximately 1.8 dB loss, reducing the maximum achievable output power.

Figure 6 shows the chip micrographs. The total areas, including pads and baluns, are 0.326 mm^2 (TB) and 0.34 mm^2 (LB).

BUILDING THE COMPLETE ON-WAFER MEASUREMENT SYSTEM

The core instrument for RF PA validation is often a VNA. This one-box instrument offers many measurement capabilities that are needed to characterize and optimize a PA. The baseline S-parameters enable the derivation of device parameters like gain,

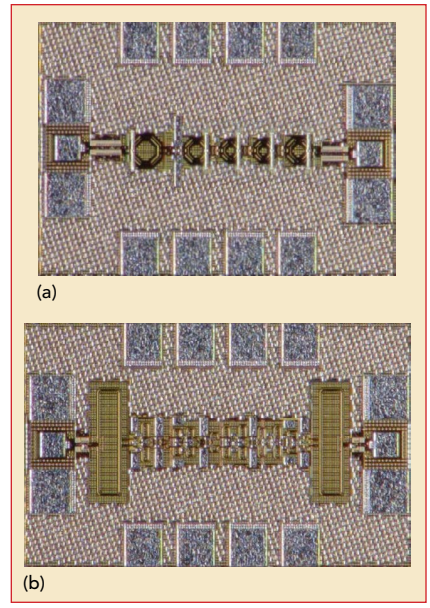

Fig. 6 **TB-PA (a) and LB-PA (b) micrographs.**

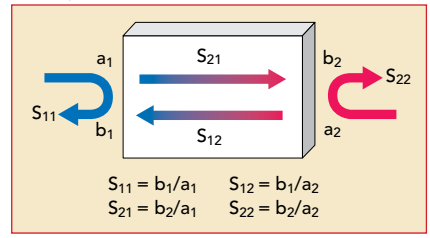

Fig. 7 **Definition of *a* and *b* wave quantities.**

gain compression, amplitude and phase distortion. Pulsed S-parameters, harmonic measurements, noise figure and intermodulation points are additional KPIs that come from an enhanced VNA with an extended feature set. If the DUT is not adequately cooled, pulsed S-parameter measurements may avoid overheating.

PAs are often used beyond their linear range to enhance power efficiency. Here, traditional small-signal S-parameters are not valid. However, a VNA can still determine the corresponding wave quantities, as shown in ***Figure 7***.

External frequency converters commonly extend VNA measurements into sub-THz frequency ranges, reaching 1.1 THz and beyond. The VNA controls the converters and the VNA user interface shows the target frequencies. ***Figure 8*** shows a VNA with external converters. External converters placed near the DUT minimize losses.

LOAD-PULL

Different impedances are pre-

Fig. 8 **ZNA VNA with mmWave converters.**

sented to the DUT input/output for comprehensive device characterization and optimization. This replicates the effect of dispersive loads, as an antenna might create. It also unveils the DUT optimization potential and the matching circuitry that optimizes gain, efficiency and other KPIs. This is important since devices behave differently under various impedances. The unpredictable behavior across different conditions requires extensive measurements to create and optimize accurate simulation models. By controlling independent parameters, the load-pull procedure allows DUT performance mapping under different impedances. The optimal performance condition can be established by plotting the DUT performance.

A common approach for creating different impedances is passive load-pull, which uses mechanical tuners to create a varying load. This approach is scalable in frequency and applicable up to 330 GHz. ***Figure 9*** displays a passive load-pull system block diagram.

Impedance tuners generate a reflection factor that can be controlled over a defined frequency range using the mechanical movement of complex loads within the tuner. In passive load tuning, the returning signal, a_2, is always smaller than the transmitted signal, b_2, because of transmission losses and tuner reflection. Therefore, the magnitude of the reflection coefficient, Γ, is always < 1 and the impedance point resides inside the Smith chart. The outer range of the Smith chart is not reachable in a pure passive load-pull system. Reducing loss in the tuner and transmission line between the DUT and the tuner enables a larger accessible Smith chart range, as shown in ***Figure 10***.

Adding frequency converters to D-Band frequencies adds complexity to the setup. To optimize the dynamic range for the receive channels of the forward and reverse waves, *a* and *b*, the tuner separates these signals on the input and output sides of the DUT. Specific down-converter receivers, shown in ***Figure 11***, measure the independent signals.

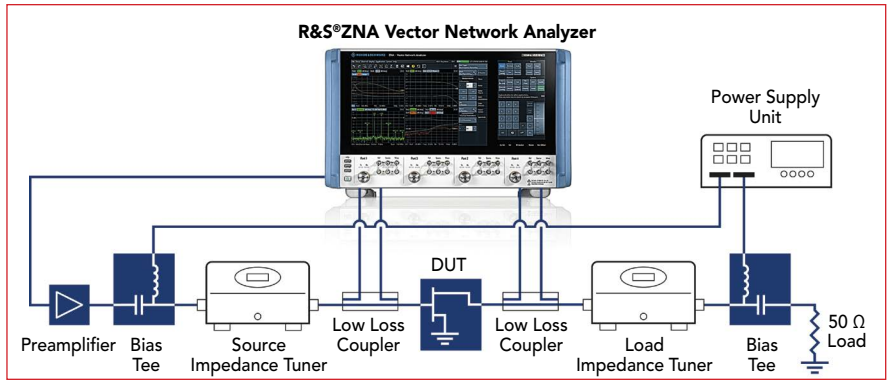

Fig. 9 **Typical passive load-pull setup.**

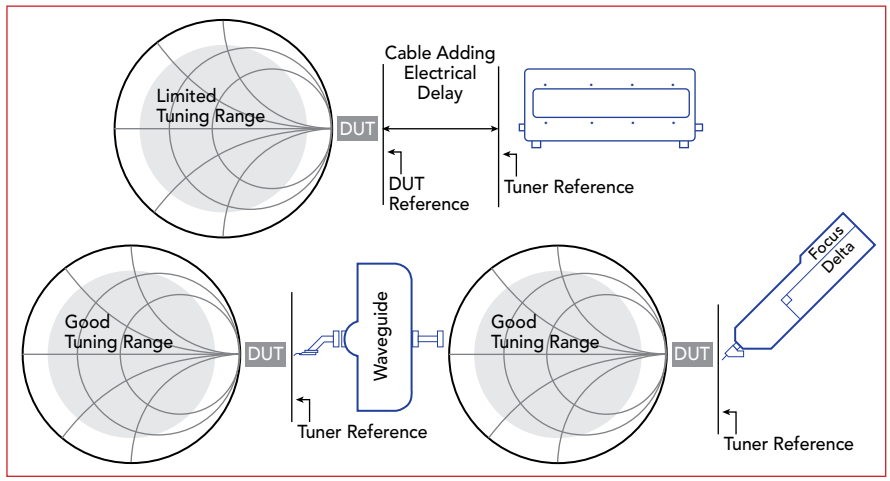

Fig. 10 **Conventional tuner structure versus Focus Delta tuner with direct RF probe connection.**

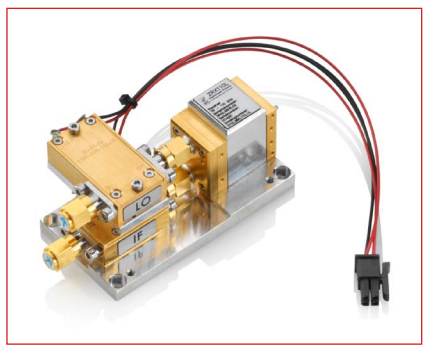

Fig. 11 **R&S ZRX170L mmWave mini receiver modules.**

Measuring the *a* and *b* waves allows the vector load-pull to calculate the real-time tuner impedances presented to the DUT. A standard converter on the DUT's input side provides the test signal. ***Figure 12*** shows the RF and IF signal flow, along with the measurement and calibration components. A second converter and power sensor are added for calibration.

COMPLETE ON-WAFER SETUP

The setup uses a probe station to contact the DUT shown in Figure 6. The challenge is to combine DC and RF probing efficiently. Precaution was taken to have similar landing pads between the two PA variants. Pads often have a combination of DC, digital and RF channels. Based on the layout, one probe needs to support the different channel functions. The MPI TITAN™ Multi-Contact Probe, which supports mixed-signal characterization requirements, shown in ***Figure 13***, handles high-density probing needs, covering pitches down to 50 µm.

As discussed, precise probe positioning is essential to minimize loss between the tuner and DUT. Direct probe connection to the tuner eliminates additional transitions. A waveguide transition is typical in this frequency range to minimize

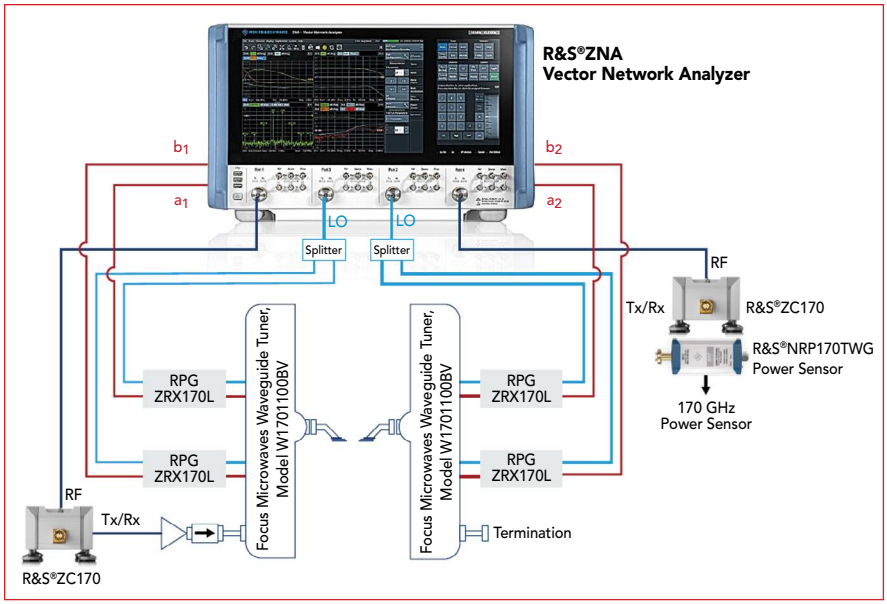

Fig. 12 **Frequency-converted load-pull system.**

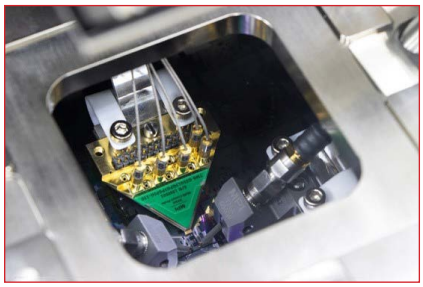

Fig. 13 **Multi-contact probe solution.**

loss while providing a stable connection without phase drift. This transition between the tuner and the mmWave receiver modules or the mmWave converter requires precise positioning. The probe station must support this to enable room for additional amplification blocks or isolators. To address mechanical constraints for this complex setup, MPI Corporation developed a four-axis positioner to support the D-Band tuner plus the measurement system components. The RF connections are on opposite sides of this configuration, while the DC/mixed-signal probes occupy the other opposite sides. MPI's large-area MP4X positioners provide support for the rigid waveguide setup, ensuring mechanical stability and minimizing phase drift during D-Band measurements for repeatable and accurate testing. ***Figure 14*** shows the test system. The screen offers an enlarged view of the DUT from the installed microscope. ***Figure 15*** shows a close-up of the DUT, probes, blue tuners,

Fig. 14 **On-wafer characterization system.**

mmWave receivers and the converters on the sides.

SYSTEM-LEVEL CALIBRATION AND CONTROL

System calibration is important for VNA measurements. There are two steps:

- Calibrate the on-wafer system with the VNA and its converters using MPI calibration solutions and the accompanying software, including test coupons as calibration standards
- Calibrate the system load-pull tuners with the Focus Microwaves software.

Once calibration is complete, the Focus Microwaves software acts as the system software. It controls the applied impedance using the tuners and the R&S ZNA to perform the RF measurements for device characterization. The MPI prober ensures stable test conditions in positioning: a cold plate and a controlled, integrated airflow within the probe station cool the DUT.

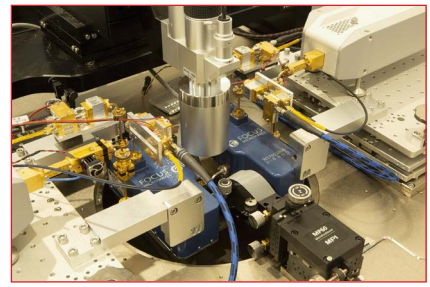

Fig. 15 **Close-up of the on-wafer system.**

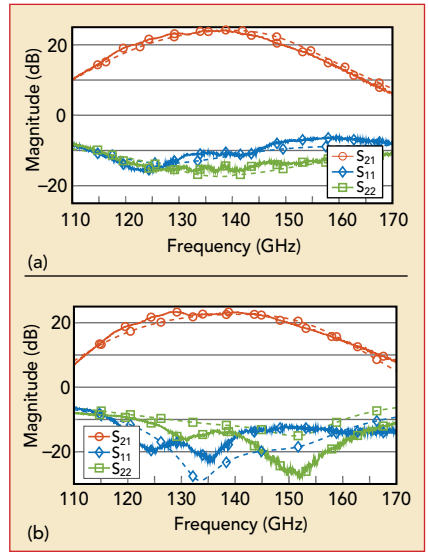

Fig. 16 **Simulated (dashed) and measured (solid) S-parameters without load pull: TB-PA (a) and LB-PA (b).**

D-BAND PA MEASUREMENTS

Engelmann et al.[4] reported validation results for two PAs without load-pull. ***Figure 16*** shows this comparison and S-parameters for TB-PA and LB-PA (including balun and pad losses). Peak small-signal gains of 24.2 and 23.4 dB with 3 dB bandwidths of 23 and 26.2 GHz around the center frequencies of 135.3 and 135.8 GHz were achieved for TB-PA and LB-PA. Both PAs have reverse isolation, S12, < -37 dB over the D-Band frequency range.

Figure 17 shows large-signal measurements without load-pull. It shows more significant deviations in saturated output and PAE, particularly for the TB-PA architecture. The PA saturation region deviation is hard to explain when analyzing only small-signal S-parameters since large-signal effects cannot be considered accurately.

As expected, the LB-PA is relatively insensitive to the load imped-

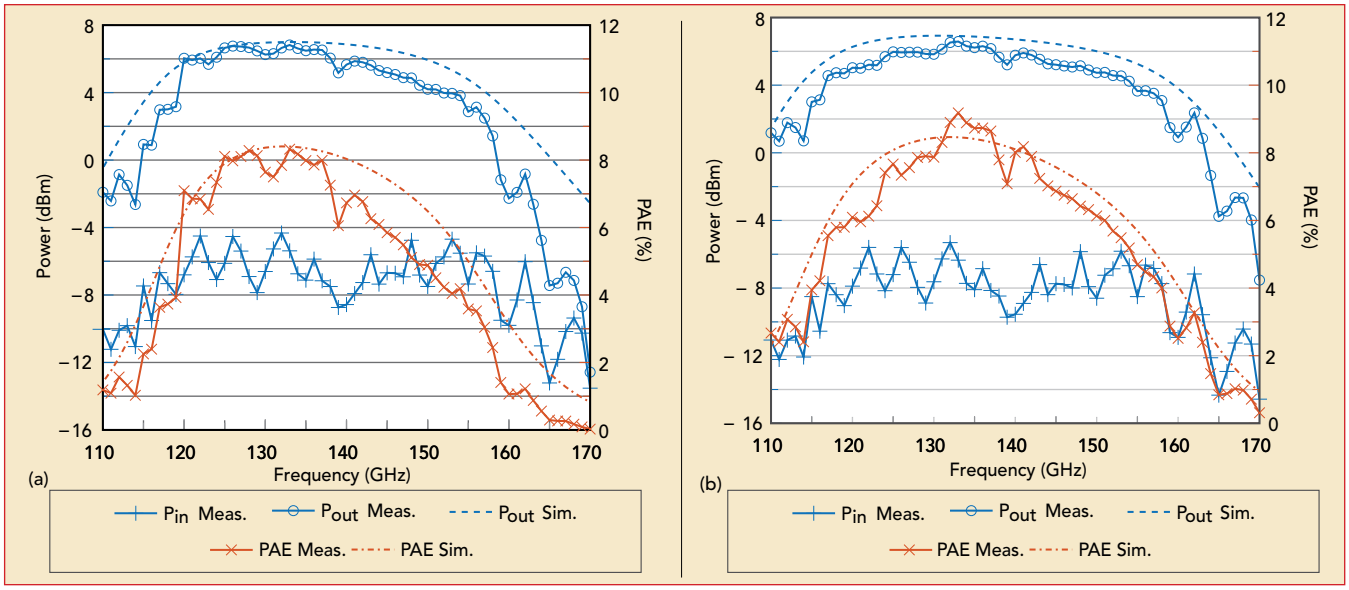

Fig. 17 Simulated (dashed) and measured (solid) P_{out} and PAE without load pull: TB-PA (a) and LB-PA (b).

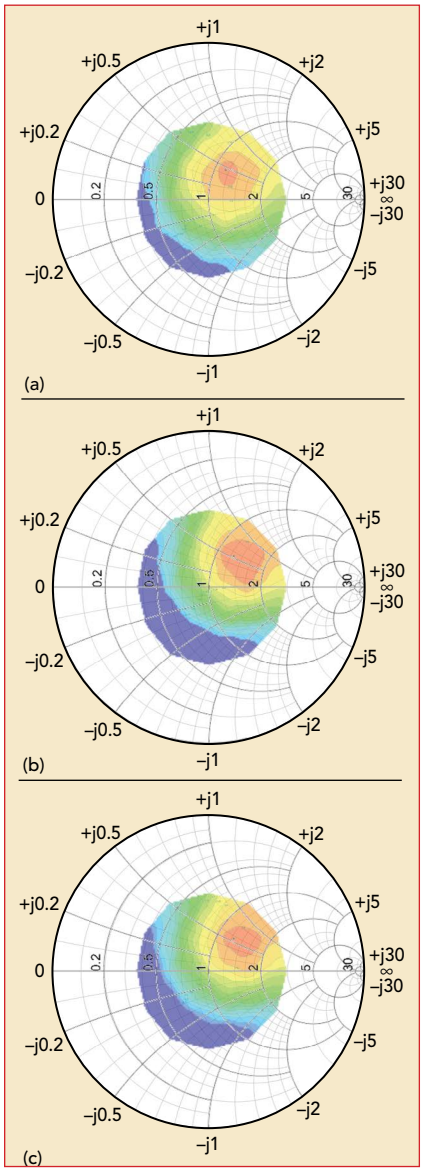

Fig. 18 LB-PA load-sensitivity measurements: (a) small signal; (b) 1 dB compression and (c) saturated.

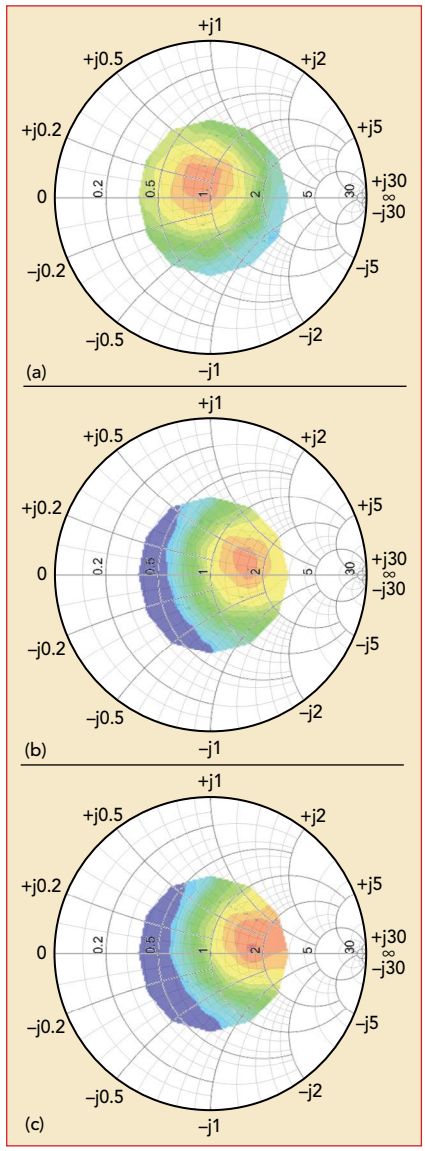

Fig. 19 TB-PA load-sensitivity measurements: (a) small-signal P_{out}; (b) saturated P_{out} and (c) saturated PAE.

ance, thanks to its output-matching network and broadband Marchand baluns. ***Figure 18*** illustrates the LB-PA P_{out} distribution as a function of the load in linear, 1 dB compression and saturated regimes.

As expected, the TB-PA load-pull measurement shows more sensitivity to load variations in ***Figure 19***. The output power contours shift drastically from the small-signal to the saturation region. The maximum small-signal output power occurs near the Smith chart's center, indicating excellent 50 Ω small-signal matching. This, however, changes with increasing output power, shown by the constant power contour shift to higher impedances. Output-matching network model inaccuracies, especially at higher frequencies, are the likely cause of the 50 Ω load not transforming to the optimum load point, Z_{opt}, for maximum achievable power. Deviations in the load-pull simulations used to determine Z_{opt} are another possibility. However, LB-PA should show similar deviations. The measurement results provide enhanced insights into the PA's large-signal behavior, which simplifies understanding the simulation-to-measurement deviations. The load-pull measurement enables better device modeling and indicates PA load sensitivity. For the PMCW PA Tx module in Figure 2, load-pull data validates whether the impedance variations of the antenna will degrade the PA output power and the overall system performance.

CONCLUSION

This article addressed the complexity of RF characterization at mmWave and sub-THz frequencies and provided an example of on-wafer D-Band amplifier measurements. Two specific PAs designed for radar sensing applications were investigated using different architectures and output-matching approaches. The example stresses the importance of accounting for load-pull when characterizing active components in the mmWave and sub-THz frequencies, particularly when looking at large-signal parameters. ■

ACKNOWLEDGMENTS

The authors would like to thank Dr. Sajjad Ahmed at Focus Microwaves and Vince Mallette at MPI Corporation for their excellent collaboration and support for the on-wafer load-pull test system. The authors want to express their gratitude to GlobalFoundries for providing silicon fabrication through the 22FDX® university program. The PA design work was initially funded and supported by the Federal Ministry of Education and Research (BMBF), Germany, through the joint research project REGGAE within the ForMikro research initiative under grant 16E106S1.

References

1. D. Simic and P. Reynaert, "A 14.8 dBm 20.3 dB Power Amplifier for D-band Applications in 40 nm CMOS," *IEEE Radio Frequency Integrated Circuits Symposium (RFIC)*, 2018, pp. 232–235.
2. J. Zhang, T. Wu, L. Nie et al., "A 120–150 GHz Power Amplifier in 28-nm CMOS Achieving 21.9-dB Gain and 11.8-dBm Psat for Sub-THz Imaging System," *IEEE Access*, Vol. 9, 2021, pp. 74 752–74 762.
3. M. Cui, Z. Tibenszky, D. Fritsche et al., "An Area Efficient 48 - 62 GHz Stacked Power Amplifier in 22nm FD-SOI," *14th European Microwave Integrated Circuits Conference (EuMIC)*, 2019, pp. 120–123.
4. A. Engelmann, P. Hetterle, F. Probst, R. Weigel and M. Dietz," Design of Two Low DC- Power High-Efficiency D-Band Power Amplifiers in 22 nm FDSOI," *17th European Microwave Integrated Circuits Conference (EuMIC)*, Milan, Italy, 2022, pp. 212–215, doi: 10.23919/EuMIC54520.2022.9923463.
5. F. Probst, A. Engelmann, M. Koch and R. Weigel," A Dual-Channel 15 Gb/s PRBS Generator for a D-Band PMCW Radar Transmitter in 22 nm FD-SOI," *IEEE Wireless and Microwave Technology Conference (WAMICON)*, 2023, pp. 129–132, doi: 10.1109/WAMICON57636.2023.10124888.